PHYSICAL REVIEW B **84**, 064427 (2011)

Thickness dependence of the magnetic properties of ripple-patterned Fe/MgO(001) films

Felix Büttner,[1,*] Kun Zhang,[1] Susanne Seyffarth,[2] Tobias Liese,[2] Hans-Ulrich Krebs,[2] C. A. F. Vaz,[3] and Hans Hofsäss[1]
[1]*II. Physikalisches Institut, Universität Göttingen, Friedrich-Hund-Platz 1, 37077 Göttingen, Germany*
[2]*Institut für Materialphysik, Universität Göttingen, Friedrich-Hund-Platz 1, 37077 Göttingen, Germany*
[3]*SwissFEL, Paul Scherrer Institut, 5232 Villigen PSI, Switzerland*

(Received 1 December 2010; revised manuscript received 8 June 2011; published 24 August 2011)

Grazing incidence Xe^+ ion sputtering was used to create a nanoscale ripple pattern on a thin Fe film, epitaxially grown on MgO(001). The Fe film has a thickness gradient of 0–20 nm and a ripple height of about 3 nm, giving rise to a transition from a continuous film to separated nanorods with decreasing film thickness. This allowed the investigation of the competition between the uniaxial and biaxial anisotropy of the irradiated sample as a function of thickness. From magneto-optical Kerr effect measurements, we determine accurately the cubic magnetocrystalline anisotropy and the uniaxial anisotropy that originates from the ripple pattern using a coherent rotation model. Our results show that the uniaxial anisotropy strength increases, whereas the contribution of the biaxial crystal anisotropy decreases, when going from the continuous film to the nanorod structures.

DOI: 10.1103/PhysRevB.84.064427 PACS number(s): 75.70.−i, 75.30.Gw, 79.20.Rf, 75.50.Bb

I. INTRODUCTION

With the rapidly decreasing size of ferromagnetic particles in various applications such as storage devices, thermal fluctuations become more and more critical for the lifetime of the magnetic state. In the superparamagnetic limit, i.e., when the magnetic anisotropy energy becomes comparable to the thermal energy, the magnetization of the particle will be randomly distributed in the absence of an external field. Hence, this particle is unable to store data. Since the rate of thermal switching events decreases exponentially with decreasing energy barrier that has to be overcome, strengthening of the magnetic anisotropy (and hence roughening the potential landscape) by nanopatterning of ferromagnetic films has attracted much attention recently.[1–4]

The formation of a nanoscale ripple pattern by ion-beam erosion is a well-known phenomenon nowadays. First observed by Navez *et al.*,[5] it was theoretically explained by Bradley and Harper.[6] With a large variety of experiments performed on different materials, ion-beam-induced self-organization can be considered a sophisticated technique for the fabrication of a periodic nanopattern.[7,8] For example, the effect of ion-beam-induced ripple patterns on the magnetic properties of ferromagnetic films has been investigated for polycrystalline Fe and Ni films by Zhang *et al.*,[9,10] for ultrathin epitaxial Co films by Moroni *et al.*,[11,12] and for monocrystalline Fe/Ag(001) films by Bisio *et al.*[13,14] and Hicken *et al.*,[15] while the magnetic anisotropies in a 20-nm-thick epitaxial Fe/MgO(001) film have been studied by Zhan *et al.* using a theoretical model for the coercivity at different sample orientations.[16] However, no systematic research has been performed to investigate the thickness dependence of the observed competition of uniaxial and biaxial anisotropy. In this work, we aim to present reliable and consistent values for the (normalized) strength of both anisotropies. To achieve this goal, we used a thermodynamic model to extract accurately the saturation energy out of hysteresis loops. It is then possible to extract the parameters of the rotation model (i.e., the anisotropy strengths and the in-plane angle of the respective easy axes) by fitting the saturation energy for different sample orientations with the theoretical model.

To study the thickness-dependent competition of the uniaxial and biaxial anisotropy, experiments have been performed on Fe films with a slight thickness gradient, epitaxially grown on MgO(001). MgO substrates were used because they are well suited for epitaxial growth and the transparent substrate allows magneto-optical Kerr effect (MOKE) measurements from the sample back side, giving us the opportunity to investigate the magnetic properties of the film near the interface with the substrate. The thickness gradient allowed us to perform ion sputtering down to a few nanometers of residual thickness without the need for an accurate *in situ* thickness determination. This thickness gradient would be difficult to achieve with a homogeneous film thickness, since the sputter yield is not perfectly known.

II. THEORY

The theoretical modeling and evaluation of the anisotropy strengths are based on the rotation model of magnetism. In this model, the total magnetization is assumed to be of constant modulus and only rotation is possible. That is, the sample is assumed to always be in a single domain state. A first-order approximation of the Gibbs free energy reads

$$G(\varphi) = K_u \sin^2(\varphi - \varphi_u) + \tfrac{1}{4} K_1 \sin^2[2(\varphi - \varphi_1)] \\ - M_s H \cos(\varphi), \qquad (1)$$

where φ is the angle between the external field and the magnetization, φ_u and φ_1 are the angles of the easy axes of the uniaxial and the biaxial anisotropy to the external field, respectively, and K_u and K_1 are the respective anisotropy constants.

Once the parameters $\varphi_u, \varphi_1, K_u$, and K_1 are known, Eq. (1) can be used to predict possible metastable states of the magnetization orientation for different external fields. Hence, it allows us to determine or verify given parameters by comparing these predictions with the actual measured loops, since we can safely assume the measured state to be thermodynamically (meta)stable. Furthermore, the shape of the predicted loops is characteristic of the rotation model; that is, we can check if the rotation model is a valid approximation in our case.

There are a number of ways to extract the anisotropy energies using MOKE measurements. A commonly used procedure is to extract these quantities out of the switching field and the slope of the hysteresis loops in a small neighborhood around it. This method uses loops which are measured with a constant magnetic field applied perpendicular to the sweeping field.[11,14,16–18] A clear advantage is that results are quickly obtained. However, there are two drawbacks. First, the anisotropy directions have to be known and cannot be extracted. Second, using only a few points of a few hysteresis loops will be less accurate than evaluating a great number of loops completely. Therefore, we decided to calculate the saturation energy E_s of the corresponding anhysteresis loop to every measured hysteresis loop as a function of the in-plane polar angle φ_H.

In the literature, the anhysteretic loop is often assumed to be just the average of both hysteresis branches.[19] However, Eq. (1) allows the calculation of local minima of the Gibbs free energy for a given external field. The weak assumption that the magnetization does not jump from one local minimum to another unless the external field is reversed, which is true for all measured loops of the epitaxial Fe films, allows a theoretical calculation of the upper branch of the hysteresis loop down to the remanent state. Such simulations reveal that the anhysteretic loop is not an average of both hysteresis branches, but instead it always follows exactly the branch of the hysteresis loop with magnetization of the highest modulus, provided that $K_u \ll K_1$, or $K_1 \ll K_u$, or $\varphi_u \approx \varphi_1 + 45^\circ$.

In our case, the first condition is fulfilled for the nonirradiated sample, while the last condition is valid for the irradiated case, given that the rod direction is along the Fe[110] direction. Hence, we can deduce the saturation energy by integrating the correct branch of the measured loops. It can be shown by computer simulation that the energy extracted this way is consistent with the one calculated by integrating Eq. (1) directly.

The anhysteretic loop can be calculated thermodynamically using

$$\mathbf{H} = \frac{\partial F}{\partial \mathbf{M}},$$

with the free energy $F = G + \mathbf{M} \cdot \mathbf{H}$. Hence,

$$\begin{aligned} E_s &= \int_{M(H=0)}^{M(H=\infty)} \mathbf{H}(\mathbf{M}) \cdot d\mathbf{M} \\ &= E_0 + K_u \sin^2(\varphi_H - \varphi_u) + \frac{1}{4} K_1 \sin^2[2(\varphi_H - \varphi_1)], \end{aligned} \quad (2)$$

where φ_h, φ_u, and φ_1 are the angles of the external field, the uniaxial, and the biaxial easy axes, respectively, with respect to a fixed sample coordinate system. The constant E_0 represents the contribution of the lower limit of the integral and is therefore isotropic.

III. EXPERIMENT

Fe grows epitaxially on MgO only under special treatment. We successfully adapted the procedure used by Lind *et al.* to grow epitaxial Fe on MgO(001).[20] The MgO substrates were first triple rinsed in trichlorethylene, acetone, and methanol. Further cleaning was performed by heating the substrates to 500 °C in the deposition chamber at a pressure of 4×10^{-8} mbar. The Fe film investigated here was grown on a MgO(001) substrate by pulsed laser deposition (PLD) with a wavelength of 248 nm, a laser fluence of 5 J cm^{-2} and a repetition rate of 10 Hz, as described earlier.[21] During deposition, the substrate was heated to 250 °C and the pressure was 5×10^{-7} mbar. Within the sample, a thickness gradient was produced by placing the substrate slightly out of the forward direction of the plasma plume.

The quality of the as-deposited sample was checked by x-ray diffraction (XRD) for the crystal structure and orientation, Rutherford backscattering (RBS) for the local film thickness and chemical purity, and atomic force microscopy (AFM) and scanning electron microscopy (SEM) for the surface topography. The magnetic properties were investigated by measuring a set of hysteresis loops as a function of the in-plane polar angle φ_H, with a step size not larger than 10° and a precision better than 0.02°.

After this first characterization, the sample was irradiated with 5-keV Xe^+ ions with an angle of 80° to the surface normal. The projection of the ion beam to the surface was parallel to the $\langle 110 \rangle$ direction of the Fe lattice. The fluence was chosen such that the film was removed on one edge of the sample while on the other edge a significant amount of Fe remained. For the relevant sample, the fluence was $1.8(2) \times 10^{17}$ $\mathrm{ions/cm}^2$. The pressure during the irradiation was 3×10^{-8} mbar. These conditions are known to be well suited for preparing nanoscale ripple patterns on polycrystalline Fe.[9,10] After the irradiation, the film was capped with a thin Cr layer to prevent oxidation.

As for the as-deposited film, the analysis of the irradiated sample was done by AFM for the ripple structure, RBS for the thickness gradient, and MOKE for the magnetic properties. All measurements were performed at various positions of the sample, covering the complete thickness interval of interest. XRD measurements were not possible due to the low residual film thickness.

A MOKE system based on a lock-in technique was used to measure the Kerr rotation.[22] To remove artifacts from the MOKE signal, a number of postmeasurement considerations were required: (i) We note that the Kerr rotation is proportional to the magnetization only to first order of approximation. In particular, if a strong crystal anisotropy is present, second order or quadratic Kerr effects are known to be significant when the external field is parallel or almost parallel to one of the hard axes of the system.[23] Since we are interested in the linear term only, we consider in the following only the antisymmetric part of the signal. (ii) The measured loops show a further contribution, which is not directly proportional to the magnetization of the film. We observe a slight constant slope in all loops, which looks like a paramagnetic contribution. This constant slope is determined using a linear fit through the high-field points of the box-shaped easy axes loops. The contribution of this constant slope is included in the error bars of the extracted saturation energy. (iii) A final correction to the calculated saturation energy is required due to the slow convergence of the magnetization to the saturation value in the rotation model. In particular, a magnetization of $0.999 M_s$ only requires a saturation energy of $0.9 E_s$, as can be calculated using Eq. (2). Since in a realistic experiment full saturation is difficult to achieve, a computational correction of

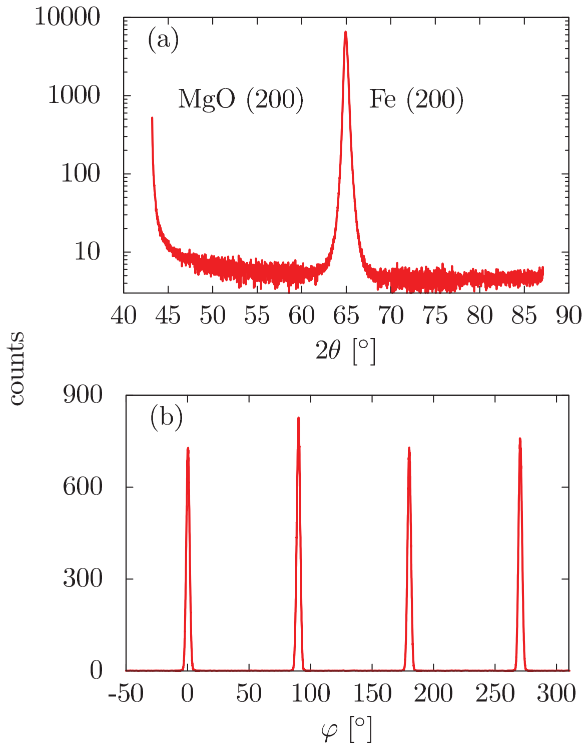

FIG. 1. (Color online) XRD measurements of the as-deposited sample. (a) Scan in Bragg-Brentano geometry, (b) φ scan of the Fe(211) planes. Both measurements verify the epitaxial structure of the iron film.

the saturation energy is carried out here. The presented data were corrected iteratively by using the saturation energy of iteration i to calculate the rotation model parameters. These parameters were used to calculate the integral in Eq. (2) for $H > H_{\max}$. This contribution was subsequently added to the saturation energy in iteration $i + 1$. The first iteration does not contain any numeric correction. The algorithm converges after a few iterations, and the result was checked by comparing the congruence between the measured data and the theoretical loop predicted by the final set of parameters.

IV. RESULTS

The crystal structure and orientation of the as-deposited Fe film was measured by XRD in the Bragg-Brentano geometry and a φ scan of the Fe(211) planes using Co-Kα radiation (see Fig. 1). In the 2θ scan it can be seen that Fe is [001] oriented. On the other hand, the φ scan of the Fe(211) planes shows a 90° in-plane symmetry. From both results it can be concluded that Fe grows epitaxially on the MgO surface with the well-known Fe(001)[110] $\parallel$ MgO(001)[100] relation due to the small lattice mismatch of about 3.8% between MgO

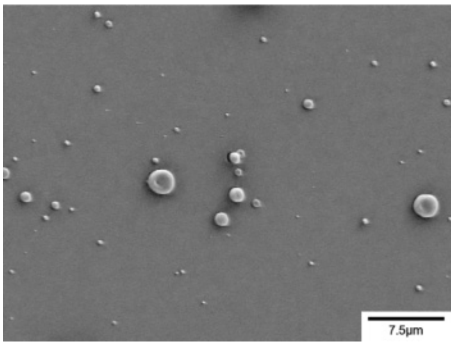

FIG. 2. SEM image of the film surface after deposition. The droplets shown here cover only 3% of the surface area and hence do not influence the MOKE measurements significantly.

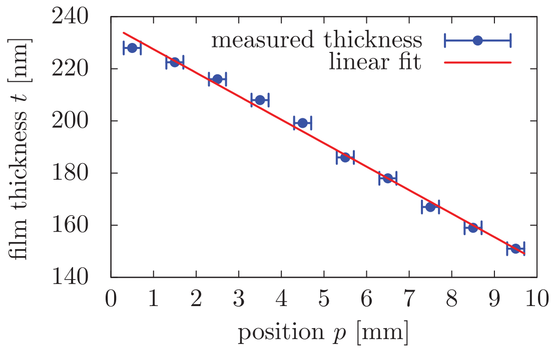

FIG. 3. (Color online) Local film thickness after deposition, determined using RBS. A perfect linear gradient with a slope of $9.0(3) \times 10^{-6}$ could be prepared.

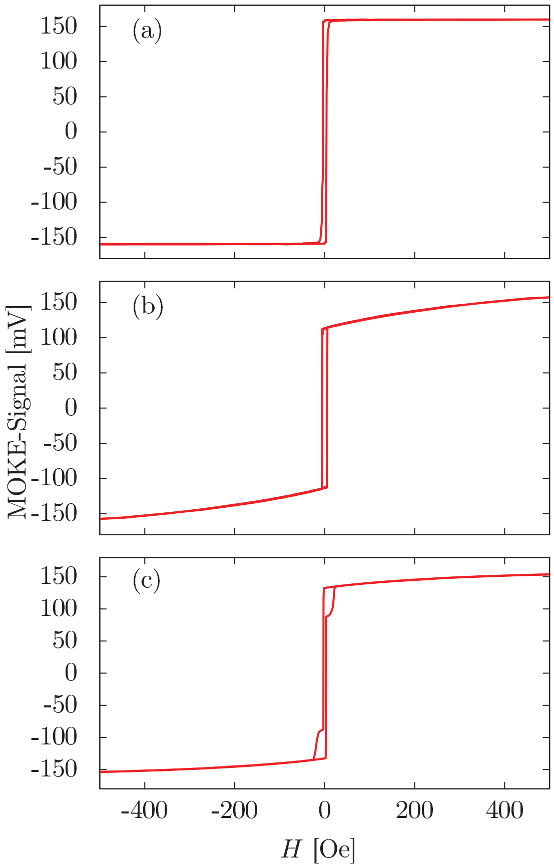

FIG. 4. (Color online) Three characteristic magnetization reversal loops of the nonirradiated sample. (a) Box-shape along the easy axis ($\varphi_H = 225°$), (b) rotation followed by a single jump along the hard axis ($\varphi_H = 272°$), and (c) rotation followed by two jumps for all angles between easy and hard axis (here $\varphi_H = 260°$)(all angles with respect to the MgO[100]$\parallel$Fe[110] axis).

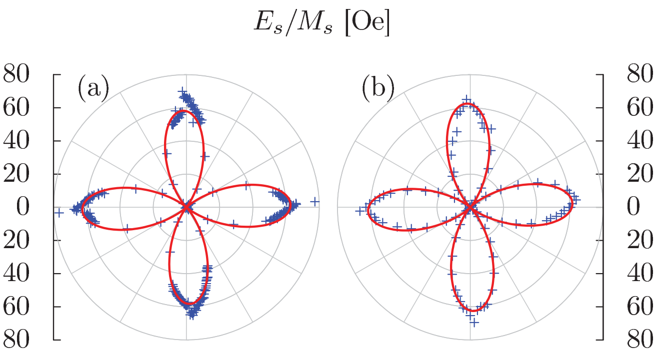

FIG. 5. (Color online) Polar diagrams of the saturation energy for (a) MOKE measurements of the film surface and (b) measurements of the interface with the MgO substrate. The symbols (crosses) are the saturation energy extracted out of the measured hysteresis loops for different in-plane orientations of the sample. The errors shown consider various uncertainties in the measurement and evaluation process. The solid line is a fit of the saturation energy according to Eq. (2).

($a = 0.4213$ nm) and Fe ($a = 0.2866$ nm) upon a 45° in-plane rotation.

Figure 2 shows a SEM image of the surface of the as-deposited Fe film. The main part of the surface is flat, with an average root-mean-square roughness of 0.38 nm, as determined by AFM. Additionally, some Fe droplets are visible, as typical for the PLD process,[21] covering a surface area below about 3% and which therefore do not significantly influence the measured magnetic properties.

The thickness gradient induced in the sample during deposition was studied by RBS. The variation of the film thickness with the position on the sample is shown in Fig. 3. It can be seen that our deposition parameters allowed us to prepare a perfect linear thickness gradient with a slope of $9.0(3) \times 10^{-6}$. Furthermore, no contamination of the film could be detected with RBS, including oxidation.

Figure 4 presents three characteristic hysteresis loops. Along one principal crystallographic axis, the clear box-shaped loop of the magnetic easy axis can be observed [Fig. 4(a)]. Along the hard axis, which is along the $\langle 110 \rangle$ directions of the Fe lattice, the hysteresis loops have a rounded shape with one jump [Fig. 4(b)]. Between easy and hard axes, the magnetization jumps twice during the reversal [Fig. 4(c)].

The anisotropy strengths can be deduced from the saturation energy. Polar diagrams of this quantity are displayed in Figs. 5(a) and 5(b) for the surface and the Fe-MgO interface of the nonirradiated sample, respectively. Both plots clearly demonstrate the fourfold magnetocrystalline anisotropy, whereas the uniaxial anisotropy usually observed in the Fe/MgO system is small.[24] The quantitative results are listed in Table I. The strength and the easy axis orientation of the biaxial (crystal) anisotropy are perfectly congruent for both measurements. The uniaxial anisotropy is not homogeneous throughout the sample. However, this may be expected since this preferred axis is most likely induced by quantities such as local stress. Figure 6 illustrates one measured hysteresis loop and the corresponding simulation that was performed with the extracted model parameters. Since both loops coincide very well, the parameters can be considered to be reliable.

TABLE I. Strength and orientation of the uniaxial and the biaxial anisotropy extracted by fitting Eq. (2) to the calculated saturation energy shown in Figs. 5(a) and 5(b). Note the much smaller uniaxial anisotropy near the Fe-MgO interface.

	K_u/M_s	φ_u	K_1/M_s	φ_1
Surface	5.0(2) Oe	78(2)°	246(1) Oe	46.7(1)°
Interface	1.5(3) Oe	158(9)°	245.6(6) Oe	47.1(1)°

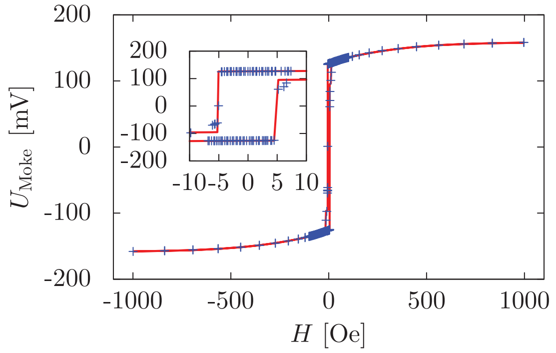

FIG. 6. (Color online) Comparison of the measured hysteresis loop for the nonirradiated film (crosses) with the theoretical prediction of Eq. (2) (solid line). The perfect agreement proves the applicability of the theory to the investigated sample.

The thickness gradient of the Fe film changes considerably upon ion-beam irradiation (Fig. 7). At a few nanometer remaining thickness, the thickness variation changed from linear to exponential and the average slope was reduced to 4×10^{-6}. The local thickness t can be described by an exponential function of the position p

$$t(p) = ae^{-bp}, \tag{3}$$

with $a = 32(4)$ nm and $b = 0.47(7)$ mm^{-1}. The correlation of the fitting parameters is $\mathrm{Cor}(a,b) = 8.6 \times 10^{-7}$. This dramatic change of the gradient shape can be understood considering the reduced sputter yield of thin films compared to bulk material of the same kind. According to Hofsäss and Zhang,[25] the sputter yield Y follows

$$Y(t) = Y_0[1 - \exp(-t/t_0)] \tag{4}$$

as a function of the film thickness t. Here Y_0 is the sputter yield of the bulk material and t_0 a characteristic thickness which is

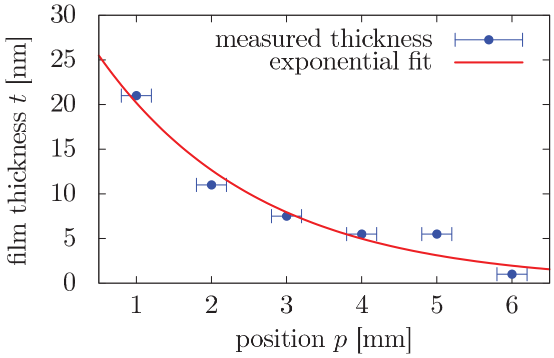

FIG. 7. (Color online) Local film thickness after irradiation.

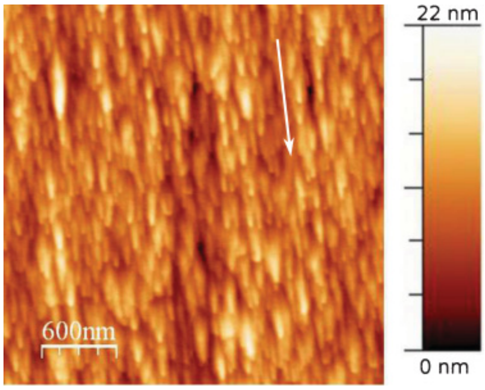

FIG. 8. (Color online) Representative AFM image of the irradiated film surface. A pronounced wave pattern can be seen with wave vector perpendicular to the projected ion-beam direction (white arrow). The AFM images were analyzed using the WSXM software version 5.0.[27]

$t_{0,\mathrm{Fe}} = 0.12$ nm for amorphous Fe on MgO (calculated with SRIM2006).[26] The strong deviation from the linear shape for thicknesses above 10 nm could be due to strong channeling effects in the epitaxial films. The bulk sputter yield is reduced to 9.4 compared to 15 for polycrystalline Fe targets. Our results indicate that the average ion penetration depth (ion ranges) and the constant t_0 are significantly larger than for polycrystalline films. The evaluation of Eq. (4) yields a characteristic thickness of $t_0 = 7(3)$ nm.

A representative AFM image of the surface topography is displayed in Fig. 8. We observe a ripple pattern with a wave vector perpendicular to the projected ion-beam direction, which is exactly what was found for polycrystalline films.[10] A constant ripple wavelength of 100(10) nm is observed over the whole film surface, and the average amplitude varies slowly as illustrated in Fig. 9. The error bars in this figure indicate the standard deviation of the ripple height distribution. From the distribution, we can calculate the percentage of valleys that touch the MgO substrate and hence separate the ripples. We see that already for $t = 3$ nm, more than 66% of the ripples are separated and therefore we have a state of separated nanorods. On the other hand, the thicker parts form a continuous film. It is of utmost interest to investigate the magnetic properties through that transition in the sample topography.

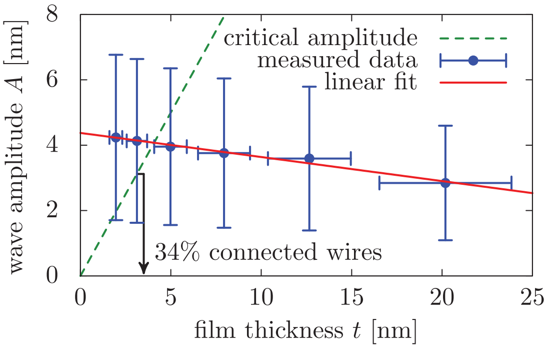

FIG. 9. (Color online) Average local ripple height and standard deviation of the height distribution as a function of the local film thickness. The critical amplitude marks the threshold for the ripple amplitude above which the valleys of the modulation touch the substrate and hence separate the rods.

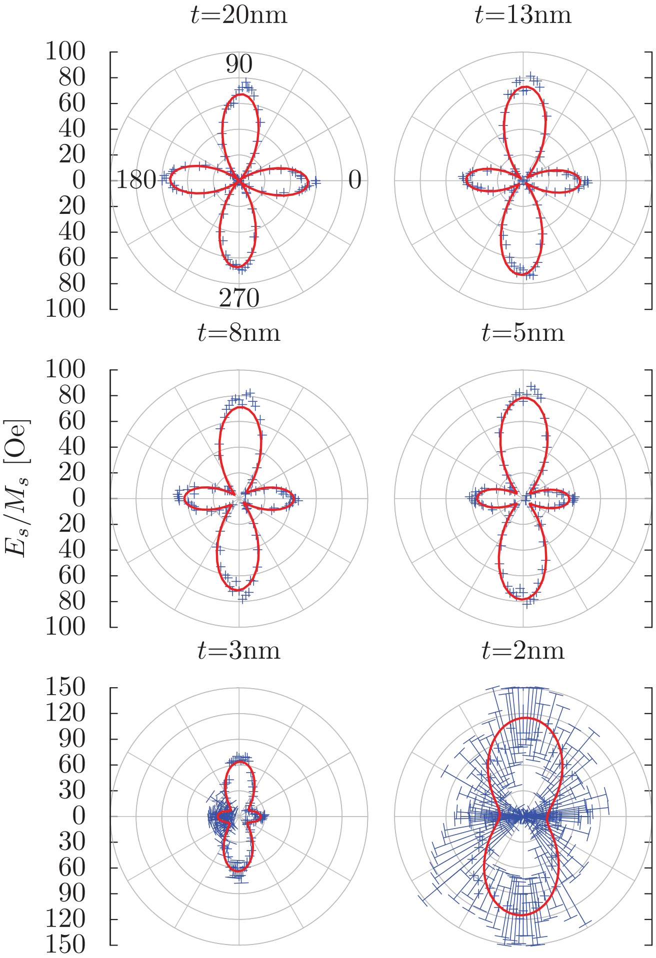

FIG. 10. (Color online) Polar diagrams of the saturation energy for different film thicknesses t probed at the film surface. The points mark the experimental data with their corresponding errors, the solid line plots the theoretical model defined by Eq. (2) fitted to the data. In the coordinate system defined in the top-left image, the ions hit the sample coming from $\varphi_H = 90^\circ$ and the crystal orientation is Fe[100]$\widehat{=}$ 45°.

In Fig. 10, the saturation energy for different thicknesses is plotted for the surface. The presence of a strong uniaxial anisotropy is evident for all measurements. The interface measurements yield similar results (as expected, due to the large penetration depth of light at 633 nm in Fe, of about 15 nm), except for small deviations that are attributed to some surface oxidation that has likely occurred in the time between the surface and the later interface measurements.

As before, we use the angular distribution of the saturation energy to fit the anisotropy parameters of Eq. (2). The results are plotted with solid lines in Fig. 10 and the agreement with the data is excellent. The same is true for the comparison of the measured loops with the modeling based on the extracted parameters (not shown). Only the thinnest layers are problematic due to the large errors. Hence, we conclude that the continuous film can be described well by the rotation model.

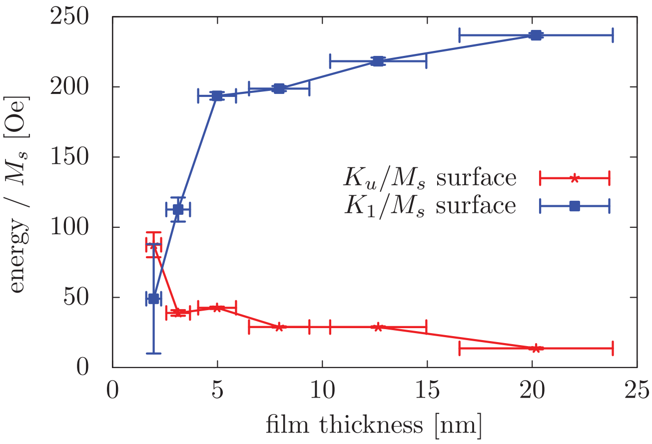

FIG. 11. (Color online) Thickness dependence of the strengths of the uniaxial and biaxial anisotropies for the film surface.

For a film thickness below 3 nm, however, we observe a smoothening of the hysteresis loops. Jumps of the magnetization are smeared out to a continuous transition of several tens of oersted width. The agreement with the rotation model becomes worse. We can understand this by considering the fact that here we have predominantly isolated nanorods. Each of these elements acts independently, each having its own individual anisotropy parameters. A large set of individual systems cannot be described by a coherent rotation model. Therefore, we cannot deduce the saturation energy accurately. This is reflected in the error bars shown. Still, even with these uncertainties, it is clear that the role of the uniaxial anisotropy becomes more pronounced at the smallest thicknesses.

The magnetic anisotropy strengths that were deduced by fitting the saturation energy are plotted in Fig. 11. In the continuous film, the normalized uniaxial anisotropy increases by a factor of 3 from 13.7(7) Oe at 20-nm film thickness to 42.6(8) Oe at 5-nm thickness. At the same time, the magnetocrystalline anisotropy decreases by 18% from 237(2) to 194(3) Oe. That is, the crystal anisotropy is still considerably larger than the ripple-pattern-induced uniaxial anisotropy. This changes at the transition to separated nanorods. While we cannot rely on the exact values of the anisotropies due to the lack of applicability of the rotation model, the dramatic drop of the magnetocrystalline anisotropy remains evident and reliable.

The influence of surface roughness on the magnetic anisotropy of a film has been studied in detail before.[28–30] In general, surface roughness leads to a decrease of the effective magnetocrystalline anisotropy strength.[28,29] Furthermore, a shape anisotropy with one preferred direction leads to the introduction of a uniaxial anisotropy.[30] Our results are in agreement with these reports. In particular, the fact that the measured effects are stronger for thinner films is a clear indication of a surface contribution. We therefore suggest that our observations of a decreasing cubic magnetocrystalline anisotropy and the onset of a uniaxial anisotropy with decreasing thickness can be explained by the directional surface roughness present in our films.

V. CONCLUSION

We have investigated the thickness dependence of the magnetic properties of epitaxial ripple-patterned films. By measuring hysteresis loops for a complete set of azimuthal angles φ_H, we could show that a coherent rotation model is capable of accurately describing the magnetic behavior of the films above a thickness of 3 nm. Consistency is shown by comparison of experimental data with simulations. Experimentally, a clear and homogeneous ripple pattern on epitaxial Fe films on MgO induced by ion-beam irradiation was found. With the layer geometry changing from a continuous film to separated nanorods, a transition from the bulk biaxial anisotropy to a dominant ripple-pattern-induced uniaxial anisotropy could be observed in the magnetic properties in tandem with a pronounced breakdown of the effective biaxial magnetocrystalline anisotropy. In summary, we have shown that the separation of the ripples and the formation of distinct nanorods lead to magnetic properties that are dominated by a uniaxial anisotropy contribution.

---

[*] felixbuettner@googlemail.com

[1] Y. Shiroishi, K. Fukuda, I. Tagawa, H. Iwasaki, S. Takenoiri, H. Tanaka, H. Mutoh, and N. Yoshikawa, IEEE Trans. Magn. **45**, 3816 (2009).

[2] D. Weller and A. Moser, IEEE Trans. Magn. **35**, 4423 (1999).

[3] V. Skumryev, S. Stoyanov, Y. Zhang, G. Hadjipanayis, D. Givord, and J. Nogues, Nature **423**, 850 (2003).

[4] J. Fassbender and J. McCord, J. Magn. Magn. Mater. **320**, 579 (2008).

[5] M. Navez, D. Chaperot, and C. Sella, C.R. Hebd. Acad. Sci. **254**, 240 (1962).

[6] R. Bradley and J. Harper, J. Vac. Sci. Technol. A **6**, 2390 (1988).

[7] G. Carter, J. Phys. D **34**, R1 (2001).

[8] U. Valbusa, C. Boragno, and F. Buatier de Mongeot, J. Phys. Condens. Matter **14**, 8153 (2002).

[9] K. Zhang, F. Rotter, M. Uhrmacher, C. Ronning, J. Krauser, and H. Hofsass, New J. Phys. **9**, 29 (2007).

[10] K. Zhang, M. Uhrmacher, H. Hofsass, and J. Krauser, J. Appl. Phys. **103**, 083507 (2008).

[11] R. Moroni, D. Sekiba, F. Buatier de Mongeot, G. Gonella, C. Boragno, L. Mattera, and U. Valbusa, Phys. Rev. Lett. **91**, 167207 (2003).

[12] D. Sekiba, R. Moroni, G. Gonella, F. B. de Mongeot, C. Boragno, L. Mattera, and U. Valbusa, Appl. Phys. Lett. **84**, 762 (2004).

[13] F. Bisio, R. Moroni, F. Buatier de Mongeot, M. Canepa, and L. Mattera, Appl. Phys. Lett. **89**, 52507 (2006).

[14] F. Bisio, A. Toma, R. Moroni, R. Pasero, F. Buatier de Mongeot, C. Boragno, M. Canepa, U. Valbusa, and L. Mattera, Phys. Rev. B **75**, 054407 (2007).

[15] R. J. Hicken, S. J. Gray, A. Ercole, C. Daboo, D. J. Freeland, E. Gu, E. Ahmad, and J. A. C. Bland, Phys. Rev. B **55**, 5898 (1997).

[16] Q. F. Zhan, S. Vandezande, C. Van Haesendonck, and K. Temst, Appl. Phys. Lett. **91**, 122510 (2007).

[17] W. Weber, R. Allenspach, and A. Bischof, Appl. Phys. Lett. **70**, 520 (1997).

[18] S. van Dijken, G. Di Santo, and B. Poelsema, Phys. Rev. B **63**, 104431 (2001).

[19] M. Brockmann, S. Miethaner, R. Onderka, M. Kohler, F. Himmelhuber, H. Regensburger, F. Bensch, T. Schweinbock, and G. Bayreuther, J. Appl. Phys. **81**, 5047 (1997).

[20] D. M. Lind, S. D. Berry, G. Chern, H. Mathias, and L. R. Testardi, Phys. Rev. B **45**, 1838 (1992).

[21] H. U. Krebs and O. Bremert, Appl. Phys. Lett. **62**, 2341 (1993).

[22] S. Polisetty, J. Scheffler, S. Sahoo, Y. Wang, T. Mukherjee, X. He, and C. Binek, Rev. Sci. Instrum. **79**, 055107 (2008).

[23] J. Hamrle, S. Blomeier, O. Gaier, B. Hillebrands, H. Schneider, G. Jakob, K. Postava, and C. Felser, J. Phys. D **40**, 1563 (2007).

[24] O. Durand, J. R. Childress, P. Galtier, R. Bisaro, and A. Schuhl, J. Magn. Magn. Mater. **145**, 111 (1995).

[25] H. Hofsss and K. Zhang, Appl. Phys. A **92**, 517 (2008).

[26] J. F. Ziegler, "SRIM: The stopping and range of ions in matter," 2006 [http://www.srim.org/].

[27] I. Horcas, R. Fernandez, J. M. Gomez-Rodriguez, J. Colchero, J. Gomez-Herrero, and A. M. Baro, Rev. Sci. Instrum. **78**, 013705 (2007).

[28] C. A. F. Vaz, S. J. Steinmuller, and J. A. C. Bland, Phys. Rev. B **75**, 132402 (2007).

[29] S. J. Steinmuller, C. A. F. Vaz, V. Ström, C. Moutafis, D. H. Y. Tse, C. M. Gürtler, M. Kläui, J. A. C. Bland, and Z. Cui, Phys. Rev. B **76**, 054429 (2007).

[30] R. Arias and D. L. Mills, Phys. Rev. B **59**, 11871 (1999).